Poly(3-dodecyl thiophene)—Organically Modified Montmorillonite Clay Nanocomposites: Influence of Chain Regioregularity and Preparation Condition on Physical, Mechanical, Optical, and Conductivity Properties

Biplab K. Kuila, Arun K. Nandi

Polymer Science Unit, Indian Association for the Cultivation of Science, Jadavpur, Kolkata 700 032, India

Received 9 January 2008; accepted 14 July 2008
DOI 10.1002/app.29074
Published online 2 October 2008 in Wiley InterScience (www.interscience.wiley.com).

ABSTRACT: The properties of regioregular(R) (98.5 mol % H-T) and regioirregular(I) (80.5 mol % H-T) poly(3-dodecyl thiophene)(P3DDT)—organically modified montmorillonite (om-MMT) clay nanocomposites obtained from solvent-cast and melt-cooled procedures are compared. The solvent-cast P3DDTI nanocomposites showed partially exfoliated clay structure but P3DDTR nanocomposites showed multistack exfoliation. Type 1 crystalline polymorph was produced in solvent-cast systems whereas melt-cooled P3DDTI samples showed mesomorphic structure. Storage modulus of P3DDTI nanocomposites increased with clay concentration showing a maximum increase of 255%. The UV-vis spectra showed blue shift of π–π^* transition band and photoluminescence spectra indicated seven times increase of normalized intensity in solvent cast P3DDTI composites. DC conductivity and *I–V* characteristic curves showed increased insulating properties with om-clay concentration. The physical, mechanical, and optical properties of P3DDTI nanocomposites are more improved than that of P3DDTR nanocomposites and from their pristine polymers. © 2008 Wiley Periodicals, Inc. J Appl Polym Sci 111: 155–167, 2009

Key words: nanocomposites; clay; poly(3-dodecyl thiophene)

INTRODUCTION

Poly(3-alkyl thiophenes) (P3ATs) are important class of conducting polymers because of their applications in different optoelectronic devices,[1] e.g., photovoltaic devices[2,3] field effect transistor,[4,5] electroluminescence,[6,7] electromagnetic shielding.[7] Besides, they are easily processible as they are fusible and soluble in organic solvents.[8] But, the physical and mechanical properties of the P3ATs are not good enough for its fruitful use in different appliances. In polymer-clay nanocomposites dramatic improvements in physical and mechanical properties are commonly observed.[9–27] In literature some report exists for the improvement of physical, mechanical, and conductivity properties of conducting polymers by making clay nanocomposites.[15–27] In this article, we would discuss the improvement of physical and mechanical properties of poly(3-dodecyl thiophene) (P3DDT), an important member of poly(3-alkyl thiophene) family, using organically modified Montmorillonite clay (om-MMT). P3ATs can be prepared for different pendant alkyl chain length and also for different regioregularity.[28–30] The physical, mechanical, and conductivity properties depend on both the alkyl chain length and chain regioregularity.[31–35] The regioregular polymers are more crystalline[32–34] and the conductivity values of regioregular samples are higher than those of regioirregular samples.[35] So it would be interesting to compare the effect of montmorillonite clay on the physical, mechanical, and conductivity properties of P3DDT for regioregular and regioirregular samples. The preparation conditions of the nanocomposites have significant effect on its physical and mechanical properties of P3HT-MMT clay nanocomposites[36,37] and this aspect will also be discussed here.

Poly(3-alkyl thiophenes) (P3ATs) are *p*-type semiconductors and exhibit photoluminescence with the holes as major carriers. The insertion and confinement of such polymer chains in quantum well

Additional Supporting Information may be found in the online version of this article.

Correspondence to: A. K. Nandi (psuakn@mahendra.iacs.res.in).

Contract grant sponsors: CSIR Grant; contract grant number: 01-(1919)/04 EMR-II.

Contract grant sponsors: Council of Scientific and Industrial Research and Department of Science and Technology under the Nanoscience and Nanotechnology Programme.

TABLE I
Characteristics of Poly(3-dodecyl thiophene) P3DDT Samples

Regioirregular P3DDT (I)	Regioregular P3DDT (R)	Montmorillonite (MMT) clay: PGV; PV-178-00
Product: Synthesized H-Tregioregularity 80.1 mol %	Product: Aldrich H-T regioregularity 98.5%	Product: Nanocor, Inc., USA
$\overline{M}_W$: 81,400	$\overline{M}_W$: 160,000	Color: white
Melting point: 67.9, 121.7°C	Melting point: 66.1, 154.8°C	Cation exchange capacity (mequiv/100 g): 101.4[a]
		Aspect ratio: 150–200
		Sp. gravity: 2.6

[a] Measured value using TGA.

usually increases photoluminescence efficiency. This is true for poly[2-methoxy-5-(2′ ethyl hexyloxy) 1,4 phenylene vinylene] (MEH-PPV) clay nanocomposites[38] but it was not the case for P3HT-clay nanocomposite produced from solvent-cast method.[36] The network supramolecular structure of the later was responsible for fluorescence quenching arising from the decay of excitons through the network junctions.[36,37] P3DDT nanocomposites may have different fluorescence property than those of P3HT because the large dodecyl pendant chains may hinder exiton transfer more than that in P3HT. Also the supramolecular structure in P3ATs depends on the alkyl chain length.[39,40] Consequently, a difference in photoluminescence behavior of P3DDT compared with that of P3HT in the nanocomposite may be possible and would be dealt here for composites produced at different condition and from different P3DDTsamples.

P3DDT exists in different polymorphic structure[41–43] due to the difference in backbone planarity controlled by the packing of side chains. In Type 1 polymorph, the pendant alkyl groups are in staggered conformation with minimal overlapping of side chains and the ordering of the side chains exist across the layer to interface.[41] In Type 2 crystal the side chains interdigitate fully to produce a planar structure.[41] Type 1 polymorph is produced from rapid evaporation of solvent of the P3AT solutions whereas Type 2 polymorph occurs from slow solvent casting of the solution. Melt cooled crystallization usually produce the noninterdigited Type 1 polymorph.[41,42] Apart from the two crystalline polymorphs P3AT also exhibit mesoporphic structure,[42–44] which is produced on slow heating of type-I crystal or from slow cooling of the melt. The mesophase is characterized by a broad X-ray peak at $2\theta \sim 20^\circ$ together with an interchain lamella distance of Type 1 polymorph.[42] The influence of om-MMT clay on the structure of nanocomposite of P3DDT (both regioregular and regioirregullar) and its dependence on processing condition would be discussed thoroughly in this article.

Finally the main aim of this work is to improve the mechanical properties, (storage modulus, loss modulus) of P3DDT without significant loss of conductivity. As P3DDT has pendant dodecyl chain so it has both β transition (T_β) temperature and glass transition temperature (T_g). The addition of clay would certainly influence the above relaxation processes and would be thoroughly discussed here. The conductivity of both undoped and iodine doped nanocomposites would be discussed here together with their characteristics *I–V* curves. All these aspects of nanocomposites are discussed giving a comparison of the properties with chain regioregularity of P3DDT and preparation condition of the nanocomposites.

EXPERIMENTAL

Materials part

Samples

Among the two P3DDT samples used in this work, the regioirregular sample (P3DDTI) was prepared from the monomer dodecyl thiophene from the $CHCl_3$ medium at 0°C using anhydrous $FeCl_3$ as initiator under nitrogen atmosphere.[45] The regioregular sample (P3DDTR) was purchased from Aldrich Chemical Co., USA. The molecular weights of the samples were measured from gel permeation chromatography (GPC, Water, USA) using THF as solvent and polystyrene as standard. The head to tail regioregularity of the samples was measured from ^1H NMR in $CDCl_3$[45] and the characteristics of the samples are presented in Table I.The MMT clay (PGV-PV-178-00, Nanocor, Arlington Height, 1 L) was organically modified by a procedure reported earlier. The exchange capacity of the clay was measured by thermogravimetric analysis and it was found to be 101.4 mequiv/100 g.[36,37]

Preparation of nanocomposite

The nanocomposites were prepared by (i) solvent cast(S) and (ii) melt-cooled (M) methods. In the former method, the om-MMT was dispersed in $CHCl_3$ (12.5×10^{-5} g cm^{-3}) and stirred with required

amount of polymer at 40°C for 3 h. The solvent was evaporated and was finally dried in vacuum at 60°C for 3 days. The nanocomposites are designated as IS1, IS2.5, and IS5 the number indicates clay percentage (w/w) in the nanocomposite. The letters I and S before the numbers stand for regioirregular P3DDT and solvent cast, respectively. For composites with regioregular samples the notation for solvent cast samples are RS1, RS2.5, and RS5.

For the preparation of melt-cooled samples, the dried solvent cast films were melted at a Metler hot stage at 160°C for 10 min and cooled to 30°C by switching off the hot stage. The process was repeated two times to ensure the complete melt mixing. The melt-cooled samples were prepared only for regioirregular P3DDT samples and they are designated as IM1, IM2.5, and IM5.

Characterization part

Wide-angle X-ray scattering study

The wide-angle X-ray scattering (WAXS) study was made from the above melt-cooled films using a Seifert X-ray diffractometer model (C 300) in reflection mode with a parallel beam optics attachment. Nickel-filtered copper Kα radiation ($\lambda = 0.154$ nm) operating at a 35 kV voltage and a 30 mA current was used. The samples were scanned from $2\theta = 1°$ to 45° at the step scan mode (step size, 0.03°, preset time, 2 s) and the diffraction pattern was recorded using a scintillation counter detector.

Transmission electron microscopy

The morphology of the PNCs was studied using a JEOL high-resolution electron microscope (model 2010EX) equipped with a CCD camera and was operated at an accelerated voltage of 120 kV. The PNCs were encapsulated in epoxy matrices and were cut into thin sections (thickness ~ 70 nm) at 25°C by an ultra cryomicrotome (Ultra R, Leica) with a glass knife. A thin section was placed on a carbon coated copper grid and was observed through the microscope. SEM study of the melt-cooled and solvent cast PNCs was made using a scanning electron microscope (JEOL GSM-5800). The samples were gold coated before observation.

Spectral characterization

The FTIR spectra of the samples were obtained from the films with a FTIR instrument [FTIR-8400S SHIMADZU]. The UV-vis spectra of the PNC films on quartz plates were taken against air at 30°C in a UV-vis spectrophotometer (Hewlett–Packard, model 8453) from 200 to 1000 nm. The photoluminescence experiments of the films were performed in a Horiba Jobin Yovon (Fluromax-3) instrument. The photoexcitation was made at an excitation wavelength of 500 nm at a 45° angle of the thin film plane. The emission was detected at a right angle to the excitation beam direction. Each spectrum was normalized with the film thickness of 1 μm for comparison purposes.

Thermal study

The melting point and enthalpy of fusion of P3DDT and nanocomposite samples were measured using a Perkin–Elmer differential scanning calorimeter (Diamond DSC) working under N_2 atmosphere. It was calibrated with indium before each set of experiment. About 3 mg sample was taken in aluminum pans and was heated at the scan rate of 10°C/min from −30 to 230°C. The melting temperature and enthalpy of fusion values were measured with the help of a personal computer using Pyris software (version 7.0).

The thermal stability of the PNCs was measured using a TGA instrument (Waters SDT Q 600) under a nitrogen atmosphere at a heating rate 10°C/min.

Dynamic mechanical property

The mechanical properties of the polymers were measured using a dynamic mechanical analyzer (DMA) (TA model Q-800). Films of 25 mm × 5 mm × 0.15 mm dimensions were made from the composites by solution casting on a die and they were installed in the tension clamp of the calibrated instrument. The samples were heated from −130 to 100°C at a heating rate of 10°C/min. The storage modulus, loss modulus, and tan δ were measured at a constant frequency of 10 Hz with a static force of 0.02 N.

dc conductivity

The dc conductivity of the samples at 30°C was measured by the standard spring loaded pressure contact four-probe method. A circular film of 1.3 cm diameter was used. A constant current (I) was passed from a constant direct current source electrometer (Keithley model 617) through two diagonal leads of the four probes and the voltage (V) across the other two leads was measured using a multimeter (Keithley, model 2000). The conductivity (σ) was calculated using van der Pauw relation

$$\sigma = (\ln 2/\pi d) \cdot (I/V) \quad (1)$$

where d, the thickness of the film was taken as the average of four measurements at different places using a screw gauge. Conductivity of two films of same sample, each with two trials, was measured and the average of four such measurements yields

the conductivity value. The samples were exposed over iodine vapor for 24 h to measure the conductivity of the doped samples.

RESULTS AND DISCUSSION

Waxs patterns

From the WAXS pattern of solvent cast P3DDTI/om-MMT nanocomposites [Fig. 1(a)] it is apparent that there are a sharp peak for $d_{hkl} = 27.0$ Å and small peaks for $d_{hkl} = 13.5$ Å of pure P3DDTI sample. This diffractogram indicates the presence of interchain lamella with the formation of Type 1 polymorph in the solvent-cast P3DDTI.[41] It is important to note that IS1 sample shows no peak or hump at lower angles except the lamellar peak but IS2.5 and IS5 samples show additional hump at $2\theta = 2.26$ and 2.34° ($d = 38$ Å), respectively, indicating the formation of exfoliated structure in the former and intercalated clay structure in the later samples. The WAXS pattern [Fig. 1(b)] of P3DDTR nanocomposites exhibit more prominent crystalline peaks for d values equal to 26.8 ($2\theta = 3.3°$), 13.5 (6.5°), 8.8 (10°), 4.5 (19.5°), 4.0 Å (22.3°) than those of regioirregular samples without the presence of any hump at lower angles as in IS2.5 and IS5 samples, [Fig. 1(a)]. These results signify that no intercalated clay structure is produced in the P3DDTR nanocomposites and also the formation of Type 1 polymorph in the composite. At lower angle, the melt-cooled samples show one additional hump apart from the P3DDT lamella peak [Fig. 1(c)] and it may arise due to the presence of intercalated clay structure. A comparison of diffractograms of the solvent cast and melt cooled P3DDTI nanocomposites indicates that the nature of higher angle diffraction pattern is different. Probably the melt-cooled samples have mesomorphic character, rather than Type 1 crystallite formation in the solvent cast samples.[42]

TEM results

In Figure 2(a–d), the TEM micrographs of P3DDT samples of different clay concentration, prepared at different conditions and of different regioregularity are presented. Figure 2(a) exhibits that IS1 has mostly exfoliated structure because the clay tactoids are oriented at different directions. Some parallel clay tactoids are also seen indicating presence of partial intercalated structure (the system has partially exfoliated clay structure). On the other hand, IS5 sample has completely intercalated structure, which is also evident from the WAXS results [Fig. 1(a)]. The melt cooled IM5 sample has also intercalated structure [Fig. 2(c)] but the micrograph of RS5 [Fig. 2(d)] indicates a different morphology

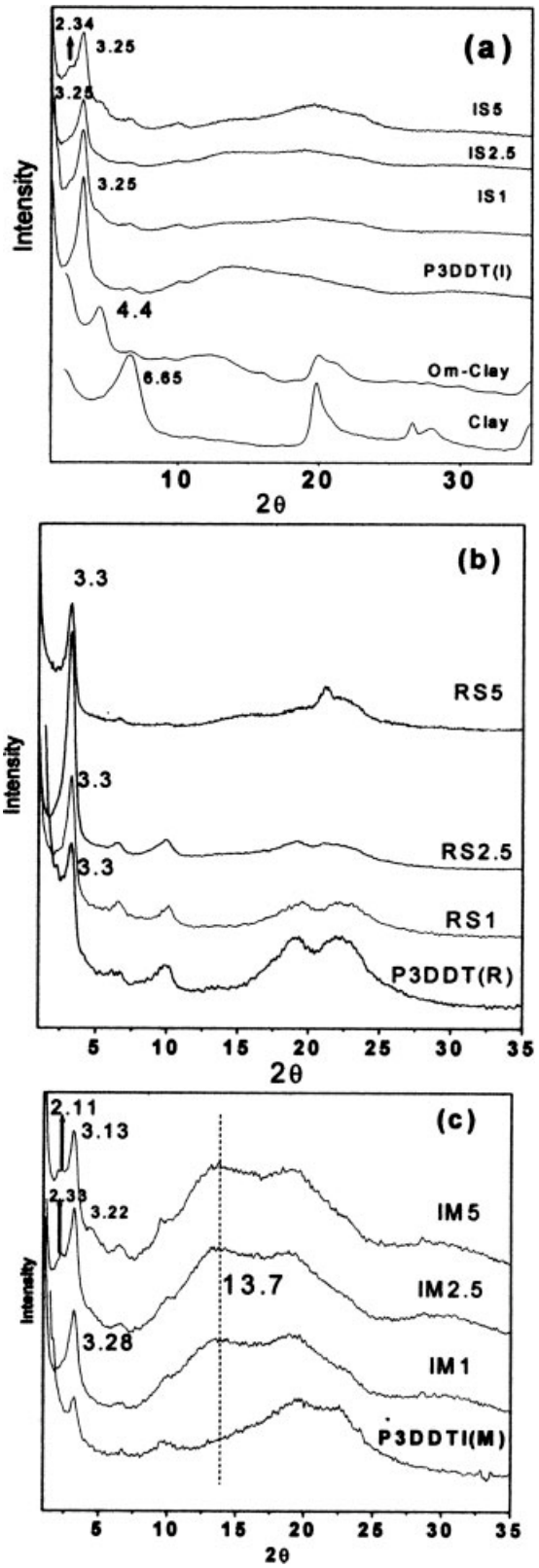

Figure 1 WAXS pattern of (a) P3DDTI, (b) P3DDTR, and (c) P3DDTIM nanocomposites prepared from solvent cast method.

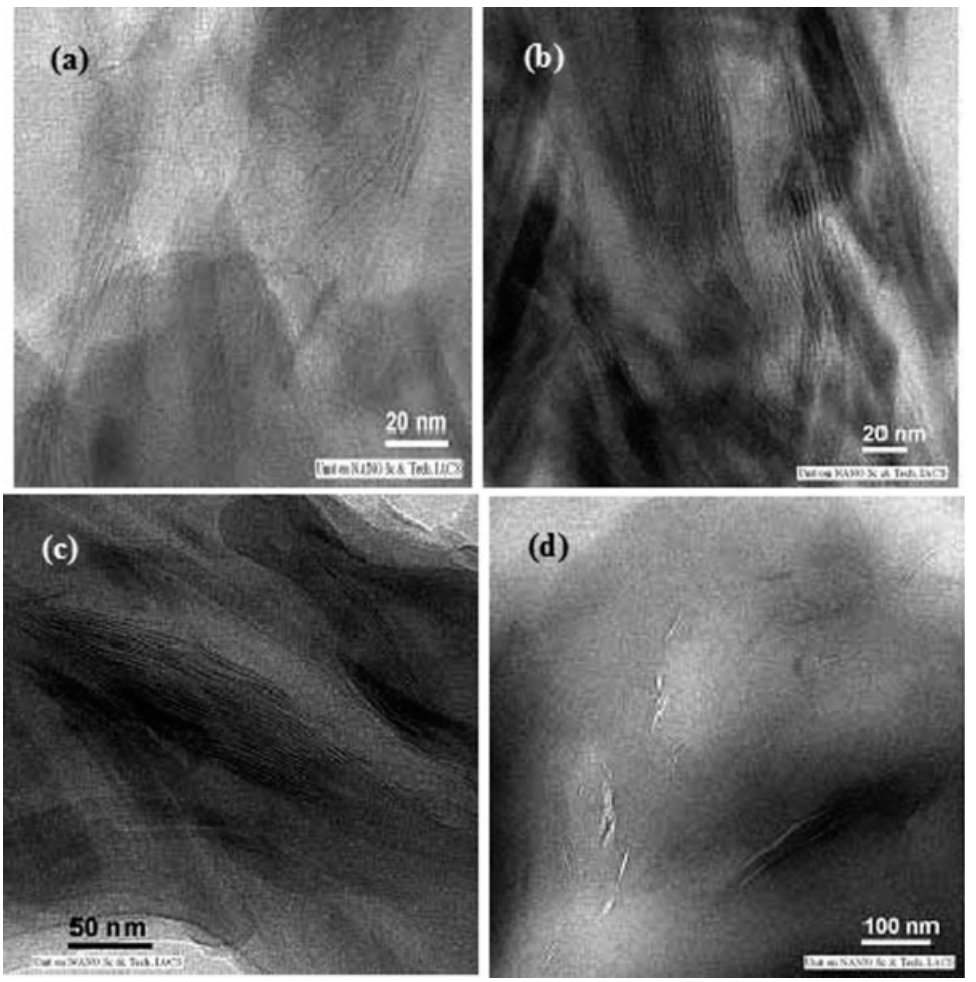

Figure 2 TEM pictures of different nanocomposites (a) IS1, (b) IS5, (c) IM5, (d) RS 5.

(bright streaks) where the clay platelets are not dispersed individually rather collectively (multistack exfoliation). This might be a reason why we do not observe any diffraction peak of intercalated clay structure in the WAXS pattern [Fig. 1(b)]. One possible reason is that the P3DDTR chains have more crystallizing force due to symmetry than that of P3DDTI chains and this force is probably higher than the attractive force of om-clay tactoids. But for P3DDTI samples, the crystallization force is lesser than its attractive force with om-clay tactoids, promoting the intercalation of the P3DDTI chains within the clay tactoids. While preparing solvent cast samples, the polymer chains in dilute solution have very low interchain interaction and also the low viscosity of the medium cause easier intercalation into the clay tactoids compared with melt-cooled samples.

FTIR results

In Figure 3, the FTIR spectra of solvent cast – P3DDTI and its nanocomposites are presented. For the om-clay 1034, 519, and 463 cm^{-1} bands are for Si—O—Si stretching, Si—O stretching and bending and the 2920, 2851, and 1470 cm^{-1} are for CH_2 asymmetric stretching, symmetric stretching, and in plane scissoring vibrations, respectively.[46,47] The 3624 cm^{-1} band is for the O—H stretching of lattice water in the clay. For P3DDTI, the 3055 and 2937–2869 cm^{-1} bands correspond to aromatic and aliphatic CH stretching, 1512 and 1464 cm^{-1} are for ring stretching, 1377 cm^{-1} is for methyl deformation, 825 cm^{-1} is for the aromatic C—H out of plane vibration and 721 cm^{-1} corresponds to methyl rocking, respectively.[30] In the PNCs, the Si—O—Si band shifts to 1026, 1030, and 1030 cm^{-1}, for IS1, IS2.5, and IS5, respectively. A probable reason for 8 cm^{-1} decrease of Si—O—Si stretching frequency in IS1 sample may be due to the partially exfoliated structure of clay tactoids where Si—O—Si stretching vibration takes place more easily than that in the lamellar state. For IS12.5 and IS5, the above frequency has increased to 1030 cm^{-1} due to the more compact nature of the intercalated state than that in the partially exfoliated state. It is, however, lesser than that of pure om-MMT indicating that the intercalated

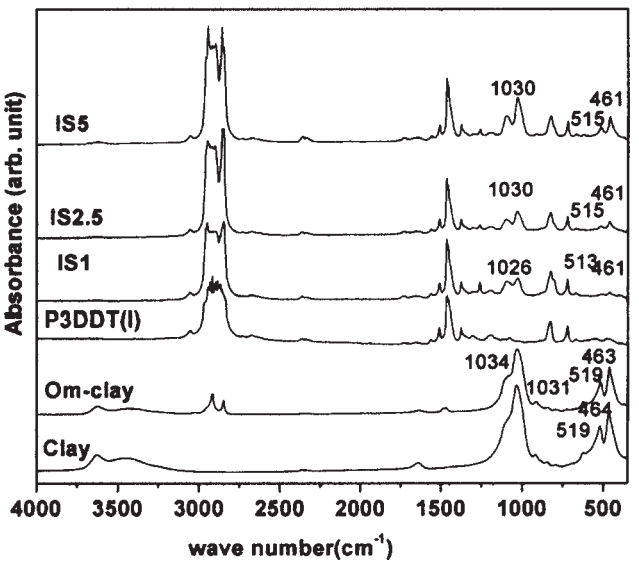

Figure 3 FTIR spectra of P3DDTI nanocomposites for indicated compositions.

P3DDT is less compact than that of om-MMT. The Si—O stretching frequencies are 519, 513, 515, and 515 cm^{-1} for pure om-MMT, IS1, IS2.5, and IS5, respectively. This decrease is also due to the decrease of compactness of clay tactoids in the PNCs, as discussed earlier. The Si—O bending frequency also decreases from 463 to 461 cm^{-1} in the PNCs due to the same reason. The 825 cm^{-1} band of aromatic C—H out of plane vibration of P3DDTI shifts to 2 cm^{-1} lower frequency in PNCs and it might be due to the increased planarity of the P3DDT chain in the PNCs. The 1261 cm^{-1} peak is a new peak in all the composites but we are at present unable to explain the cause of its appearance.

In the solvent cast P3DDTR and its nanocomposite quite different phenomenon is observed [Supp. Info. Fig. 1 (a)]. The Si—O—Si band positions of the nanocomposites remain unaltered at 1034 cm^{-1}. The Si—O stretching frequency of the PNCs is 518, 517, and 517 cm^{-1} for RS1, RS2.5, and RS5 samples, respectively, indicating Si—O stretching vibration frequency remains almost invariant. The Si—O bending vibration frequency remains also same at the values 461, 461, and 463 cm^{-1}. The reason of above results may be the strong crystallization force of regioregular P3DDTR chains than that of P3DDTI chains in the nanocomposites lowering the degree of intercalation. In the IM nanocomposites, the Si—O—Si stretching frequencies are 1032, 1032, and 1030 cm^{-1} for IM1, IM2.5, and IM5, respectively, which are slightly lower than that of pure om-clay sample [Supp. Info. Fig. 1(b)]. Possibly intercalated structure of the clay tactoids in the PNCs is the cause of such lower decrease. The Si—O stretching frequencies are 513, 513, and 515 cm^{-1} and Si—O bending frequencies are 459, 461, and 461 cm^{-1} with increasing clay concentration. Thus the decrease in Si—O—Si and Si—O frequencies in the melt-cooled state is lower than that of solvent cast PNCs, indicating dispersion of clay tactoids in the melt-cooled samples are not as good as in solvent cast samples. The higher viscosity and cohesive force of the polymer chains in the melt might be a reason for its lower degree of intercalation within the clay tactoids than that of the solvent cast samples.

Thermal properties

Thermogravimetric analysis

Figure 4 shows the TGA thermograms of IS samples and it is apparent that there is a decrease of degradation temperature with increase in om-clay concentration. The onset of degradation temperatures are 452.3, 447.3, 446.9, and 437.5°C for P3DDTI, IS1, IS2.5, and IS5, respectively. The enhancement of thermal stability is common in the PNCs[10,36] but a decrease of thermal stability in the PNCs is also reported by others.[37,48,49] In the P3DDTR nanocomposite, the degradation temperatures are 454.5, 454.5, 454.1, 453.7°C for P3DDTR, RS1, RS2.5, and RS5 [Supp. Info. Fig. 2(a)], respectively, indicating that the thermal stability of P3DDTR remains unaltered in the nanocomposites. The difference in behavior might be due to the multistack exfoliation of the clay tactoids arising from the higher crystallization force of P3DDTR chains as discussed earlier. In the melt-cooled samples, the degradation temperature of P3DDTIM, IM1, IM2.5, and IM5 are 452.3, 451.6, 446.7, and 444.5°C, respectively, [Supp. Info. Fig. 2(b)]. The degradation temperatures are almost comparable with those of the solvent cast samples. A decrease in degradation temperatures in all these

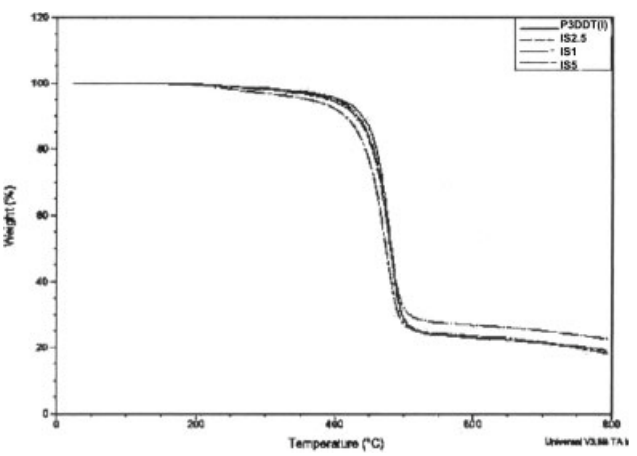

Figure 4 TGA thermograms of solvent cast P3DDTI and its nanocomposites for indicated compositions.

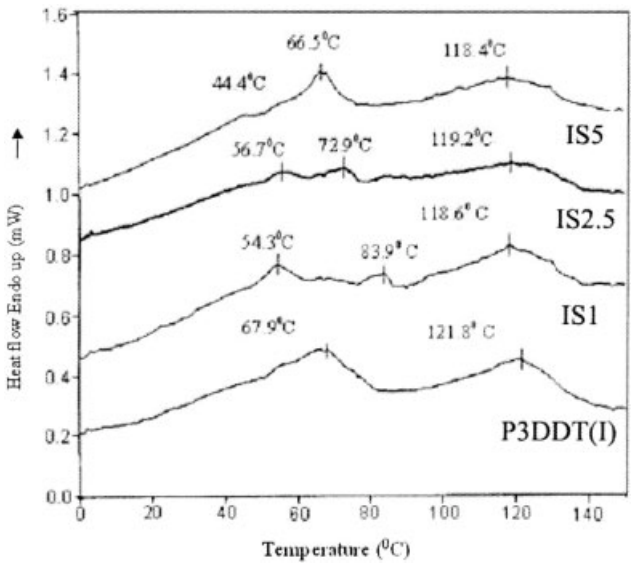

Figure 5 DSC thermograms of P3DDTI nanocomposites for indicated compositions.

systems might be due to the contact of clay tactoids with the P3DDT side chains, which easily degrades through heat transfer from the clay contacts.

DSC study

Figure 5 shows the DSC thermograms of P3DDTI and its nanocomposites produced from solvent cast method. In pure P3DDT, there are two peaks at 67.9°C and 121.8°C, which can be characterized as melting of side chains and main chain crystals, respectively.[31–34,42,50,51] It is interesting to note that on addition of clay the side chain-melting peak is bifurcated into two peaks at 54.3 and 83.9, 56.7 and 72.9, and 54.5 and 66.5°C for PNCI-1, PNCI-2.5, and PNCI-5, respectively. One possible way to explain the bifurcation of side chain melting peak is that the side-chain crystallization occurs in two ways in the nanocomposites, (i) formation of new mixed lamella of side chains of P3DDTI and the pendent chains of om-clay tactoids and (ii) formation of side chain crystals of P3DDTI in its own interchain lamella. The identification of the melting peaks from P3DDTs own side chains and mixed side chains peak is difficult. We propose that the lower side chain melting peak is for own side chain crystal of P3DDTI and the higher side chain melting peak is for the mixed side chain crystal of P3DDTI and organoclay.

The above assertion may be supported from the argument that at lower om-clay concentration the cetyl side chains interdigitate well with the dodecyl chains of P3DDTI and the higher om-clay concentration increases such side chain crystals. But in the higher om-clay concentration, the cetyl side chains may suffer from conformational irregularity causing the mixed side chain crystals to have lower melting point though the melting enthalpy increases due to the higher concentration of mixed side chain crystals. On the other hand, the melting of polymer's own side chain crystals occurs at much lower temperature (<∼ 14°C) in the PNCs and the lowering may happen due to the miscibility of side chains in the solution state.[52,53] The melting points of the main chain crystals are 121.7, 118.6, 119.2, and 118.4°C for P3DDTI, IS1, IS2.5, and IS5, respectively, indicating a gradual small decrease with increasing clay content. This suggests that the mixing of clay and polymer at the solution occurs due to the side chain interactions. In the solvent-cast P3DDTR nanocomposites [Supp. Info. Fig. 3(a)] we do not observe any splitting of the side chain crystal's melting peak. The peak temperatures also remain almost invariant in the nanocomposites indicating no significant interaction between the clay and P3DDTR and it is also supported from the FTIR data presented above. In the melt-cooled samples [Supp. Info. Fig. 3(b)], the side chain melting points are 49.9, 53.3, 54.3, and 54.5°C for P3DDTIM, IM-1, IM-2.5, IM-5 samples, respectively. This indicates that there is a gradual increase, though small, of side chain melting point with increasing om-clay concentration. It is really interesting that in the melt-cooled samples no bifurcation takes place-indicating the formation of mixed side chain crystals are not distinct. It might be possible that here mixed side chain crystals are produced in lower concentration; consequently its melting peaks become mixed and overlapped with that of the self-side chain crystals, yielding higher overall melting peak temperature. The main chain-melting peak, however, remains unaltered in the PNCs. The difference in melting behavior between the solvent-cast and melt cooled PNCI samples is probably due to the lower viscosity of the solution which allows the mixing of the side chains of polymer and clay tactoids well producing higher amount of mixed side chain crystals than that in the melt cooled samples.

Dynamic mechanical properties

The storage modulus (G'), loss modulus (G''), and Tan δ plots of solvent-cast P3DDTI samples are presented in Figure 6(a–c). It is apparent from Figure 6(a) that G' decreases with increase in temperature (T) though the decrease is not exactly linear. The loss modulus temperature plots exhibit a peak at (∼ −40°C) and a hump at (∼ −15°C). The former corresponds to β transition arising from the onset of side chains' motion, whereas the later is called as glass transition (T_g) arising from the onset of segmental Brownian

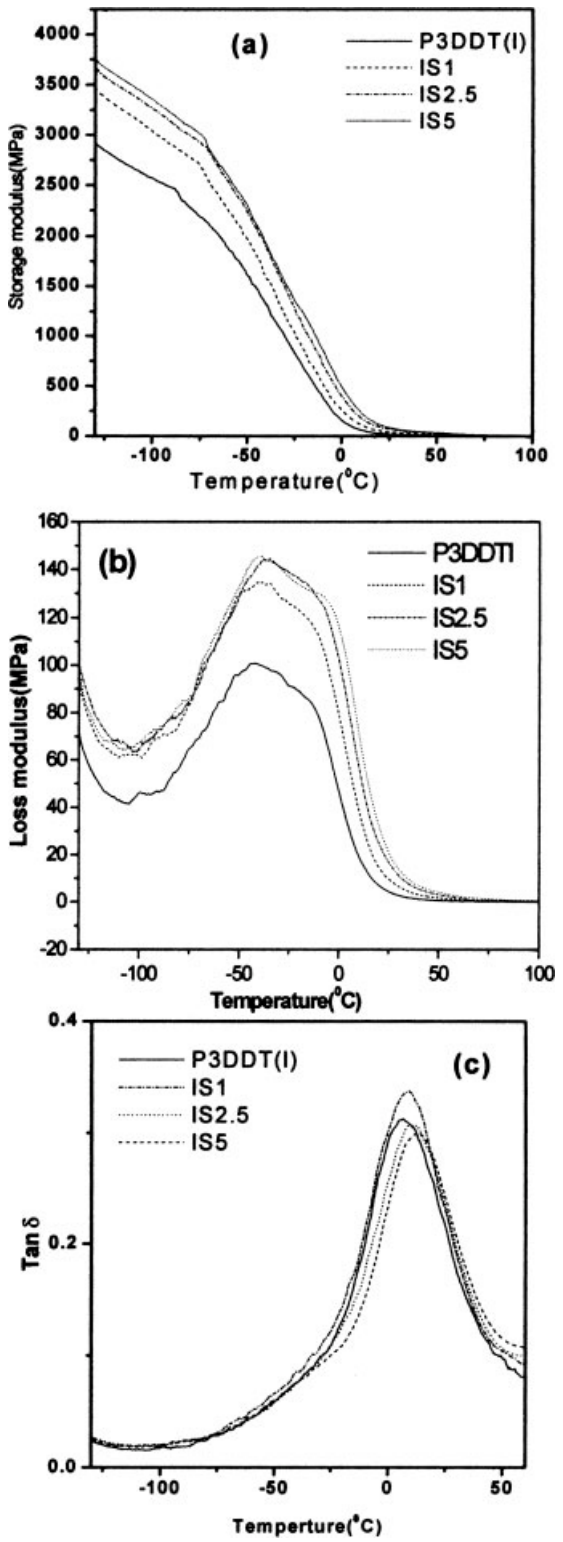

Figure 6 Dynamic mechanical property variation of P3DDTI nanocomposites with temperature (a) storage modulus, (b) loss modulus, (c) tan δ.

motion of the main chain.[33,34,36,37] Also another small hump at much lower temperature (∼ −90°C) is observed in all the solvent cast P3DDT(I) samples and it might be related to the γ transition temperature (T_γ) arising from the bond rotation of terminal methyl group of the dodecyl side chains.[54] The T_g, T_β, and T_γ transition temperatures together with G' values are presented in Table II. T_g increases linearly with increase in clay concentration whereas both T_β and T_γ shows a maximum value for IS2.5, samples. The increase of T_g with increasing clay concentration may be attributed for the increased compactness of the sample due to attractive forces of dispersed clay tactoids and to start the segmental Brownian motion of the main chain it requires larger amount of energy. The same argument is true for the other transitions in the nanocomposites except the IS5 sample. The peak temperatures of tan δ plot [Fig. 6(c)] are 6.5, 9.2, 10.9, and 13.0°C which are ∼ 22° higher than the T_g values obtained from loss modulus plot. This difference in the T_g values is due to the use of two different modes of measurement: one is from the dissipation of energy as heat (loss modulus) and the other is related to the reduction of vibration of the material, i.e., damping (tan δ).

At the glassy region, the storage modulus values are very high (Table II) but the percent increase of storage modulus due to addition of clay at these temperatures are not significant. The percent increase increases with increase in temperature and it is maximum at 0°C. Here we observe a maximum of 209% increase on storage modulus for IS5 samples. The maximum increase of storage modulus at 0°C might be due to the viscoelastic region where the reinforcement property of nanoclay is very significant. In rubbery state, the movement of chain segments is relatively free. So the reinforcement effect of clay tactoids is more effective making a higher increase in storage modulus.[55,56] The storage modulus, loss modulus, and tan δ plot of IM are presented in Supporting Information Figure 4(a–c). The T_g value increases gradually (Table III) with increasing clay concentration due to increased compactness of the sample as discussed earlier. From the Table III it is apparent that storage modulus decreases with increase in temperature but it increases with increase in clay concentration at each temperature. The highest increase (255%) is observed at 0°C, i.e., in the viscoelastic region of the sample for 5% om-clay concentration. In comparison with the solvent cast sample here the percent increase is somewhat higher which might be attributed for the more compact nature of the melt-cooled samples than that of the solvent cast samples. It is to be noted that the G', G'' and tan δ plot for P3DDTR nanocomposites could not be measured because of brittleness of the sample. This is probably due to the high crystallinity of the sample arising from the significant amount of regioregularity (98.5 mol %) in the P3DDTR chain.

TABLE II
Summary of Mechanical Properties of Solvent Cast Composites (IS) Measured by DMA

				Storage modulus (MPa)					
Sample	T_γ[a] (°C)	T_β[a] (°C)	T_g[a] (°C)	–100°C	(%) increase	–50°C	(%) increase	0°C	(%) increase
P3DDTIS	−98.8	−42.4	−17.2	2579	–	1596	–	159	–
IS1	−97.3	−37.3	−17.1	3040	17.8	1976	23.8	265	66.6
IS2.5	−84.5	−35.5	−11.2	3263	26.5	2220	39.09	402	152.8
IS5	−91.3	−37.6	−7.9	3357	30.1	2303	44.2	498	209.4

[a] From loss modulus peaks.

UV-vis spectra

In Figure 7(a,b), the UV-vis spectra of P3DDT-nanocomposites are compared for solvent cast P3DDTI and P3DDTR samples. The former exhibit an absorption peak at 513 nm corresponding to the π–π* transition of the conjugated chain.[57,58] In the IS1 it shows a blue shift of 8 nm but for 2.5 and 5% clay the peak occurs at 511 nm showing a blue shift of 2 nm only. The large blue shift in IS1 sample may be due to the partially exfoliated nature of clay tactoids. The specific attraction of the exfoliated clay tactoids induces rigidity, which wrinkle the polymer chains decreasing the conjugation length of P3DDT. So delocalization of π electrons is reduced showing blue shift in the UV-vis spectra. As the IS2.5 and IS5 samples have intercalated clay structure, so the intertactoidal cohesive attraction is lower than IS1 sample causing almost same absorption peak as in pure P3DDT. In the melt cooled P3DDTI nanocomposites, the UV-vis spectra (Supp. Info. Fig. 5) behave similar to the solvent cast samples, the highest blue shift (9 nm) occurs for 1% clay whereas the IM2.5 and IM5 show a blue shift of 3 nm only. The P3DDTR sample shows UV-vis spectra which is somewhat different from the regioirregular sample. Here the π–π* transition of the conjugated chain occurs at 524 nm and has two humps at 552 and 597 nm due to vibronic coupling. The 11 nm red shift in the pure P3DDTR sample compared with that of the P3DDTI sample arises due to the increased planarity, which increases the conjugation length. In sharp contrast to P3DDTI nanocomposites, the solvent cast P3DDTR samples do not exhibit any significant blue shift (∼ 2 nm) with the addition of clay in the UV-vis spectra [Fig. 7(b)]. This may be due to the multistack exfoliation of the clay tactoids that is occurring for faster interchain crystallization of P3DDT in the highly regioregular samples.

Photoluminescence

In Figure 8(a–c), the photoluminescence spectra of solvent cast P3DDTI, P3DDTR, and melt cooled P3DDTI nanocomposites are presented. From the Figure 8(a) it is apparent that solvent cast P3DDTI shows a luminescence peak at 664 nm and the normalized photoluminescence intensity of PNCs increases by 5–7 times than that of pure P3DDTI depending on the amount of clay in the composite. The IS5 exhibit the highest luminescence intensity. This is really an interesting and important observation and the cause of such large increase of normalized photoluminescence intensity may be due to the clay tactoids, which hinder the interchain decay of excitons. IS2.5 and IS5 have intercalated structure, so a single P3DDT chain may exist in the gallery of clay tactoids.

As a result the Forster energy transfer would be difficult and the higher energy excitons migrate into lower energy state along the same chain causing photoluminescence intensity enhancement. Also the path length of the exciting beam increases through

TABLE III
Summary of Mechanical Properties of Melt-Cooled (IM) Composites Measured by DMA

			Storage modulus data (MPa)					
Sample	T_β[a] (°C)	T_g[a] (°C)	–100°C	(%) increase	–50°C	(%) increase	0°C	(%) increase
PDDTIM	−38.3	−15.9	3317	–	2152	–	257	–
IM1	−36.1	−16.5	4526	36.4	2964	37.7	403	56.9
IM2.5	−41.2	−15.5	4914	48.1	3301	53.39	647	151.7
IM5	−39.13	−9.98	6174	86.1	4190	94.7	914	255.0

[a] From loss modulus peaks.

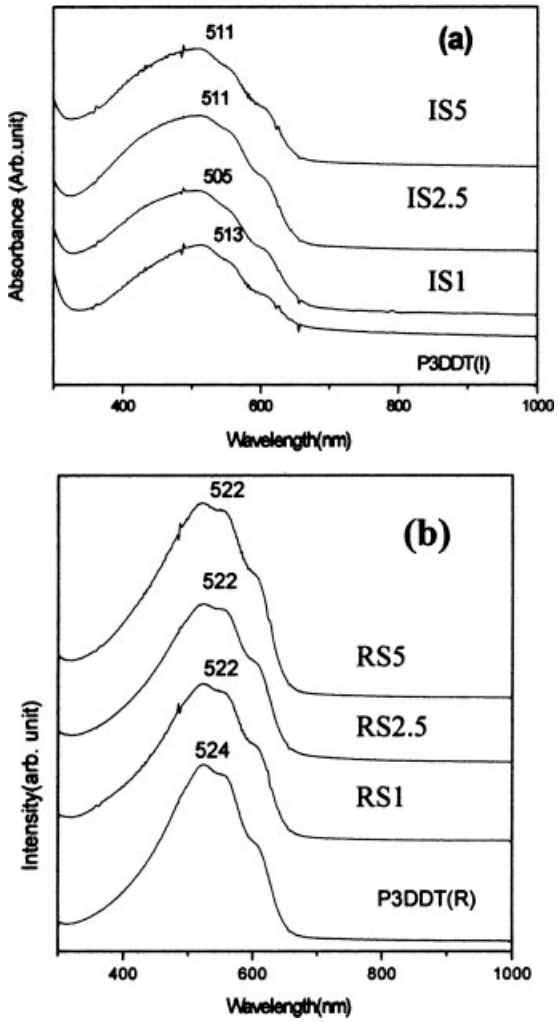

Figure 7 UV-vis spectra of solvent cast (a) P3DDTI and (b) P3DDTR nanocomposites for indicated compositions.

reflection in the clay tactoids in the intercalated structure, resulting in photoluminescence enhancement. This observation is quite different from the solvent cast P3HT om-clay nanocomposite and is similar to that of melt-cooled P3HT-om clay nanocomposites.[36,37] However, in the later case, there was a maximum of 2.5 times increase in the photoluminescence enhancement[37] but in this system the maximum enhancement is much larger ($\sim$ 7 times). Probably, the longer nonconducting side chain in P3DDT hinders the interchain exciton transfer more than that in P3HT. It is to be noted that another hump at higher wavelength (716 nm) is observed in the photoluminescence spectra of the composite probably due to two different paths of energy transfer. In the solvent cast P3DDTR -om-clay nanocomposites [Fig. 8(b)] somewhat different behavior is observed. Here the emission of P3DDTR occurs at 657 nm and the photoluminescence quenching occurs for RS1 samples whereas RS2.5 and RS5 exhibit photoluminescence enhancement by 2.5 times. The reason of photoluminescence enhancement is same as discussed earlier. The lower degree of photoluminescence enhancement in P3DDTR nanocomposites than that of regio-irregular P3DDT might be due to the multistack exfoliation of clay tactoids where the polymer chains are not well separated as in P3DDTI sample. In Figure 8(c) the photoluminescence behavior of the melt cooled P3DDTI-clay

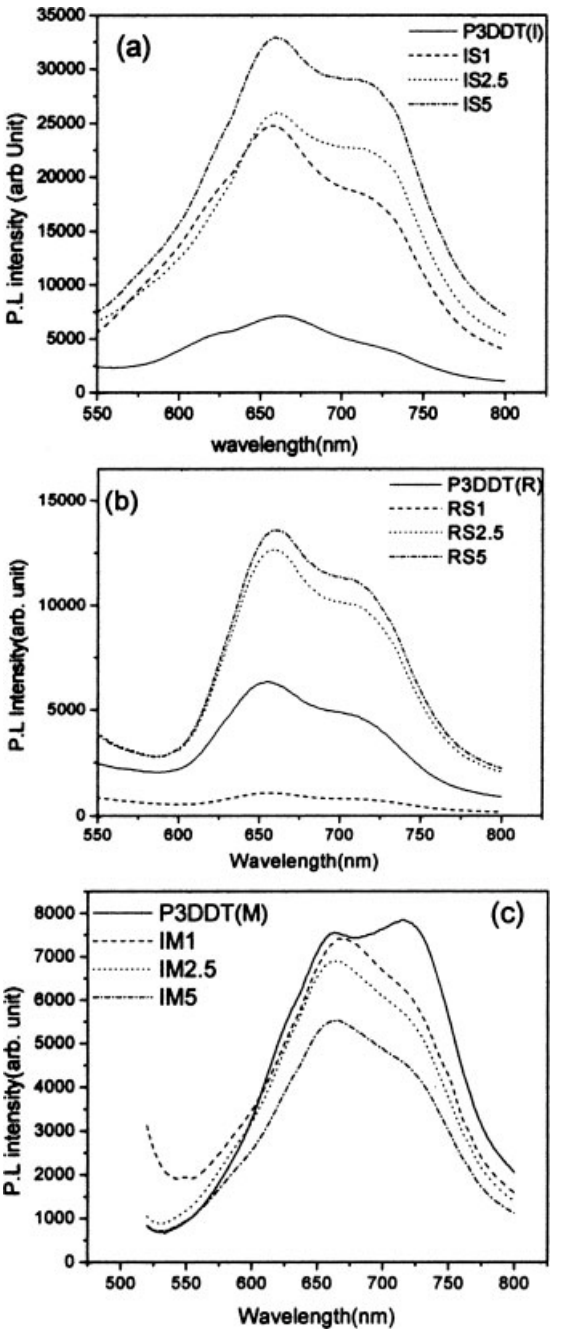

Figure 8 Photoluminescence spectra of P3DDT nanocomposites after excitation by radiation of 490 nm wavelength (normalized to film thickness of 1 μm) (a) P3DDTI, (b) P3DDTR, (c) P3DDTIM nanocomposites.

TABLE IV
Conductivity (σ) Values (S/cm) of Different Nanocomposites

	P3DDT (I) solvent cast		P3DDT(I) melt cooled		P3DDT(R) solvent cast	
Sample % clay	Undoped $\sigma \times 10^{-6}$	I_2 doped $\sigma \times 10^{-2}$	Undoped $\sigma \times 10^{-7}$	I_2 doped $\sigma \times 10^{-3}$	Undoped $\sigma \times 10^{-4}$	I_2 doped $\sigma \times 10^{-2}$
P3DDT	2.06	1.55	6.3	9.90	3.82	4.28
1%	0.59	0.33	0.32	3.67	1.35	3.89
2.5%	0.45	0.14	0.25	3.24	1.21	3.87
5%	0.44	0.09	0.12	2.08	0.68	2.29

nanocomposites are presented. Here quenching in photoluminescence is observed in the nanocomposites and greater the clay concentration larger is the quenching. The quenching in the melt cooled P3DDTI samples having intercalated structure is really an exception and no definite reason can be afforded here. A probable reason of quenching may be thought from a comparison of the normalized intensity values of solvent cast and melt cooled P3DDTI samples [cf. Fig. 8(a,c)]. The P3DDTIM has 1.5 times greater fluorescence intensity than that of solvent cast P3DDTI sample. The formation of mesomorph in the melt cooled condition might cause a decrease of exciton decaying paths than those of Type 1 crystallites of solvent-cast samples as the excitons can decay through the side chain crystallites easily. This decrease of decaying paths in mesomorphic structure causes a $\sim$ 1.5 times enhancement of photoluminescence intensity. On addition of clay some ordering in mesomorphic structure occurs as evident from an additional hump in WAXS pattern [Fig. 1(c)] at $2\theta = 13.7^\circ$. This short range order might be responsible for the formation of additional decaying paths causing a fluorescence quenching. This effect is quite large as it nullifies the fluorescence enhancement effect of intercalated structure [Fig. 8(a)] and causes a resultant decrease in the fluorescence intensity.

dc conductivity and *I–V* characteristic curve

The dc conductivity values of the nanocomposites are presented in Table IV for solvent cast P3DDTI, P3DDTR, and melt cooled P3DDTIM samples in undoped and iodine-doped form. It is apparent from the table that the conductivity of P3DDTI samples increases by four orders after doping but for P3DDTR samples the increase is only two orders. Both for undoped and doped systems, the conductivity decreases by an order in the PNCs of all categories except P3DDTR nanocomposites where the conductivity decrease is negligible. The conductivity decrease may be explained from the increased band gap as evident from the blue shift of π–π^* transition band of PNCs in the UV-vis spectra (Fig. 7). In the P3DDTR nanocomposites, the blue shift is also negligible causing almost unchanged conductivity. In the undoped state, the dc conductivity of P3DDTR nanocomposites are two orders higher than that of P3DDTI samples but in the doped state the conductivity is only one order higher.

The current–voltage (I-V) characteristic curves of the solvent cast P3DDTI-om-MMT nanocomposite are presented in Figure 9(a). It is evident from the figure that pure P3DDTI has good semi conducting property but it decreases abruptly with the addition of om-clay. For the PNCIM samples, the *I–V* curve is somewhat wavy in nature, however, with addition of clay the wavy nature decreases and the nanocomposites exhibit more insulating property. The *I–V* characteristic curves of P3DDTR-clay nanocomposites remain almost same for the small addition of clay [e.g., RS1 and RS2.5 sample] though the RS5 sample exhibits a small decrease in semiconductivity. From the *I–V* plots it can be concluded that PNCR nanocomposites are better semiconductor than that of PNCI nanocomposite samples.

CONCLUSIONS

The solvent cast P3DDTI-om-clay nanocomposites exhibit exfoliated clay structure below 2.5% (w/w) clay concentration and above that intercalated clay structures are produced. The melt cooled P3DDTI-om clay nanocomposites, however, exhibit intercalated clay structure at all compositions. In the solvent cast samples, Type 1 crystalline polymorph is produced whereas the melt cooled samples exhibit mesomorph like characteristics. The DSC endotherms of solvent cast P3DDTI nanocomposites exhibit two side chain melting peaks probably arising from the melting of pure and mixed side chain crystals of P3DDTI and om-clay tactoids. The addition of om-clay increase the storage modulus and the increase of G' is greater in melt-cooled samples than that in solvent cast samples. The UV-vis spectra of both solvent cast and melt cooled samples of P3DDTI-nanocomposites exhibit blue shift due to decrease of conjugation length for the induced rigidity from the cohesive attraction of clay tactoids. A maximum of seven times increase of normalized photoluminescence intensity is

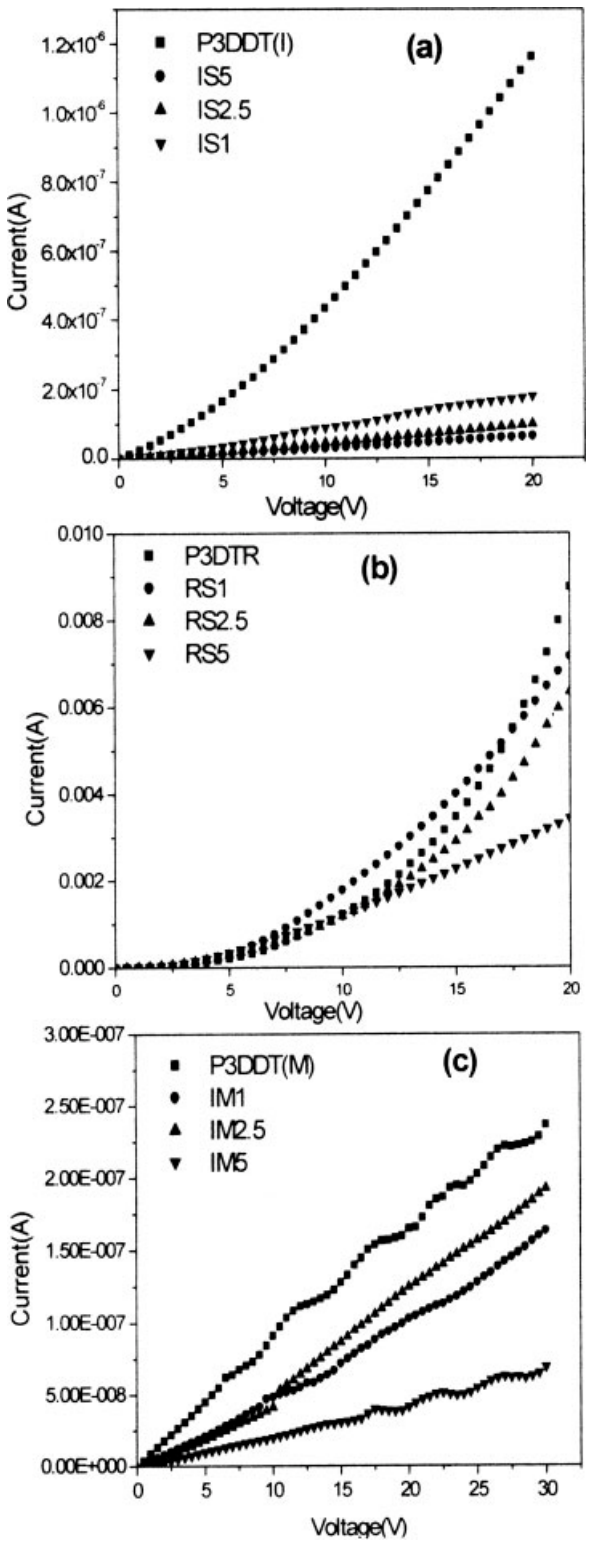

Figure 9 *I–V* characteristic curve of (a) P3DDTI, (b) P3DDTR, and (c) P3DDTIM nanocomposites.

observed in the solvent cast PNCI5 sample but for the melt cooled PNCs photoluminescence quenching occurs. The dc conductivity decreases with increase in clay concentration and the conductivity of melt-cooled PNCs are one order lower than that of solvent cast PNCs. The *I–V* characteristic curves indicate a decrease in semiconducting properties of the nanocomposites with increasing om clay concentration in both the systems.

Compared with regioirregular P3DDT samples, the regioregular P3DDT samples exhibit different properties in the nanocomposites. Here multistack clay exfoliation rather than the exfoliation or intercalation of clay tactoids is observed. No appreciable change in WAXS, FTIR, TGA, DSC, and UV-vis results in the nanocomposites from that of pure P3DDTR. In the solvent-cast P3DDTR nanocomposites, the normalized photoluminescence intensity shows a maximum of 2.5 times increase than that of pure sample compared with seven times increase in the regioirregular nanocomposites. In the undoped state, the dc conductivity of P3DDTR nanocomposites are two orders higher than that of regioirregular samples but in the doped state the conductivity is only one order higher. This study therefore concludes that regioirregular poly(3-alkyl thiophene) nanocomposites exhibit better enhancement in mechanical and photoluminescence properties than that of the regioregular samples.

References

1. McCullough, R. D.; Ewbank, P. C. In Hand Book of Conducting Polymers, 2nd ed.; Skotheim, T. A.; Elsebaumer, R. L., Reynolds, J. R., Eds.; Marcel Dekker: New York, 1998; p 225.
2. Bhattacharyya, S.; Kymakis, E.; Amartunga, G. A. J Chem Mater 2004, 16, 4819.
3. Liu, J.; Tanake, T.; Surula, K.; Alvistos, A. P.; Fretchet, J. M. J. J Am Chem Soc 2004, 126, 6550.
4. Babel, A.; Jenekhe, S. A. Macromolecules 2003, 36, 7759.
5. Salleo, A.; Chen, T. W.; Vokel A. R.; Wu, Y.; Liu, P.; Ong, B. S.; Street, R. A. Phys Rev B 2004, 70, 115311.
6. Endo, T.; Rikukawa, M.; Sanui, K. Synth Met 2001, 119, 191.
7. Kossmehl, G.; Engelman, G. In Handbook of Oligo and Poly Thiophenes; Fichon, D., Ed.; Wiley-VCH: Weinheim, 1999; p 491.
8. Roncali, J. Chem Rev 1992, 92, 711.
9. Giannelis, E. P.; Krishnamoorty, R.; Manias, E. Adv Poym Sci 1999, 138, 107.
10. Vaia, R. A.; Krishnamoorti, R. In Polymer Nanocomposites: Synthesis Characterization and Modeling; Krishnamoorti, R.; Vaia, R. A., Eds.; American Chemical Society: Washington, D. C., 2001; p 1.
11. Okamoto, M.; Morita, S.; Kim, Y. H.; Kotaka, T.; Tateyama, H. Polymer 2001, 42, 1201.
12. Maiti, P.; Nam, P. H.; Okamoto, M.; Hasegawa, N.; Usuki, A. Macromolecules 2002, 35, 2042.
13. Fornes, T. D.; Yoon, P. J.; Keskkula, H.; Paul, D. R. Polymer 2001, 42, 9929.
14. Alexandre, M.; Dubois, P. Mater Sci Eng Rev 2000, R28 (1–2), 1.
15. Choi, H. J.; Kim, J. W.; Joo, J. Synth Met 2001, 121, 1325.
16. Do Nascimento, G. M.; Constantino, V. R. L.; Temperini, M. L. A. Macromolecules 2002, 35, 7538.
17. Kim, J. W.; Liu, F.; Choi, H. J.; Hong, S. H.; Joo, J. Polymer 2003, 44, 289.
18. Davis, H. C.; Mathias, L. J.; Gilman, J. W.; Schiraldi, D. A.; Shields, J. R.; Trulove, P.; Sutto, T. E.; Delong, H. C. J Polym Sci Part B: Polym Phys 2002, 40, 2661.

19. Do Nascimento, G. M.; Constantino, V. R. L.; Landers, R.; Temperini, M. L. A. Polymer 2006, 47, 6131.
20. Hoang, V. H.; Holze, R. Chem Mater 2006, 18, 1976.
21. Ballav, N.; Biswas, M. Synth Metals 2004, 142, 309.
22. Moujahid, El M.; Dubois, M.; Besse, J.-P.; Leroux, F. Chem Mater 2005, 17, 373.
23. Fang, F. F.; Choi, H. J.; Joo, J. J Nanosci Nanotechnol 2008, 8, 1559.
24. Ballav, N.; Sardar, P. S.; Ghosh, S.; Biswas, M. J Mater Sci 2006, 41, 2959.
25. Boutaleb, N.; Benyoucef, A.; Salavagione, H. J.; Belbachir, M.; Morallon, E. Eur Polym J 2006, 42, 733.
26. Salavagione, H. J.; Cazorla-Amoros, D.; Tidjane, S.; Belbachir, M. Benyoucef, A. Morallon, E. E. Eur Polym J 2008, 44, 1275.
27. Do Nascimento, G. M.; Constantino, V. R. L.; Landers, R.; Temperini, M. L. A. Macromolecules 2004, 37, 9373.
28. Neimi, V. M.; Knuuttila, P.; Osterholm, J. E.; Korvela, J. Polymer 1992, 33, 1559.
29. Mc Cullough, R. D.; Lowe, R. D.; Jayaraman, M.; Andersson, D. J Org Chem 1993, 58, 904.
30. Chen, T.-A.; Wu, X.; Rieke, R. D. J Am Chem Soc 1995, 117, 233.
31. Malik, S.; Nandi, A. K. J Polym Sci Part B: Polym Phys 2002, 40, 2073.
32. Pal, S.; Nandi, A. K. Macromolecules 2003, 36, 8426.
33. Pal, S.; Nandi, A. K. J Phys Chem B 2005, 109, 2493
34. Pal, S.; Nandi, A. K. Polymer 2005, 46, 8321.
35. Pal, S.; Roy, S.; Nandi, A. K. J Phys Chem B 2005, 109, 18332.
36. Kuila, B. K.; Nandi, A. K. Macromolecules 2004, 37, 8577.
37. Kuila, B. K.; Nandi, A. K. J Phys Chem B 2006, 110, 1621.
38. Lee, T.-W.; Park, O. O.; Kim, J. J.; Hong, J.-M.; Kim, Y. C. Chem Mater 2001, 13, 2217.
39. Malik, S.; Jana, T.; Nandi, A. K. Macromolecules 2001, 34, 275.
40. Malik, S.; Nandi, A. K. J Appl Polym Sci 2007, 103, 2528.
41. Prosa, T. J.; Winokur, M. J.; Mc Cullough, R. D. Macromolecules 1996, 29, 3654.
42. Bolognesi, A.; Pozio, W.; Zhuo, G.; Ezquerra, T. Eur Polym J 1996, 32, 1097.
43. Meille, S. V.; Romita, V.; Caronna, T.; Lovinger, A. J.; Catellani, M.; Belobrzeckaja, L. Macromolecules 1997, 30, 7898.
44. Tashiro, K.; Ono, K.; Minagawa, Y.; Kobayashi, M.; Kawai, T.; Yoshino, K. J Polym Sci Part B: Polym Phys 1991, 29, 1223.
45. Amou, S.; Haba, O.; Shirato, K.; Hayakawa, T.; Uede, M.; Takeuchi, K.; Asai, M. J Polym Sci Part A: Polym Chem 1999, 37, 1943.
46. Zeng, Q. H.; Wang, D. Z.; Yu, A. B.; Lu, G. Q. Nanotechnology 2002, 13, 549.
47. Darder, M.; Colilla, M.; Ruitz-Hitzky, E. Chem Mater 2003, 15, 3774.
48. Yeh, J. M.; Liou, S. J.; Lin, C. Y.; Cheng, C.-Y.; Chang, Y.-W.; Lee, K.-R. Chem Mater 2002, 14, 154.
49. Yeh, J. M.; Liou, S.-J.; Lai, C.-Y.; Wu, P.-C.; Tsai, T.-Y. Chem Mater 2001, 13, 1131.
50. Park, K. C.; Levon, K. Macromolecules 1997, 30, 3175.
51. Liu, S. L.; Cheng, T. S. Polymer 2000, 41, 2781.
52. Nishi, T.; Wang, T. T. Macromolecules 1975, 8, 909.
53. Maiti, P.; Nandi, A. K. Macromolecules 1995, 28, 8511.
54. Ferry, J. D. Viscoelastic Properties of Polymers, 3rd Ed.; Wiley: Singapore, 1980; p 449.
55. Roy, S. S.; Maiti, P.; Okamoto, M.; Yamado, K.; Ueda, K. Macromolecules 2002, 35, 3104.
56. Usuki, A.; Kawasumi, M.; Kujima, Y.; Okada, A.; Kurauchi, T.; Kamiginto, O. J Mater Res 1993, 8, 1185.
57. Rughooputh, S. D. D. V.; Hotta, S.; Hegger, A. J.; Wudl, F. J Polym Sci Part B: Polym Phys 1987, 25, 1071.
58. Liu, Y.; Xu, Y.; Zhu, D. Macromol Chem Phys 2001, 202, 1010.